Hindawi
Journal of Nanomaterials
Volume 2020, Article ID 1508574, 11 pages
https://doi.org/10.1155/2020/1508574

Research Article

Ion-Exchanged ZIF-67 Synthesized by One-Step Method for Enhancement of CO_2 Adsorption

Fujiao Song,[1] Yan Cao,[1] Yunxia Zhao,[2] Ruiyu Jiang,[3] Qi Xu,[1] Jinlong Yan ,[1] and Qin Zhong[4]

[1]*School of Environmental Science and Engineering, Yancheng Institute of Technology, Yancheng 224051, China*
[2]*Jiangsu Collaborative Innovation Center of Atmospheric Environment & Equipment Technology, Jiangsu Key Laboratory of Atmospheric Environment Monitoring and Pollution Control, School of Environmental Science and Engineering, Nanjing University of Information Science & Technology, Nanjing 210044, China*
[3]*Key Laboratory for Advanced Technology in Environmental Protection of Jiangsu Province, Yancheng Institute of Technology, Yancheng 224051, China*
[4]*School of Chemical Engineering, Nanjing University of Science and Technology, Nanjing 210094, China*

Correspondence should be addressed to Jinlong Yan; 1448313363@qq.com

Received 15 October 2019; Accepted 4 December 2019; Published 17 February 2020

Academic Editor: Dong Kee Yi

Copyright © 2020 Fujiao Song et al. This is an open access article distributed under the Creative Commons Attribution License, which permits unrestricted use, distribution, and reproduction in any medium, provided the original work is properly cited.

Li^+- and Na^+-exchanged ZIF-67 was synthesized by a new one-step method of ion as-exchange technique and tested as CO_2 adsorbents. As a comparison, the standard ion-exchange procedure was also carried out. The powder X-ray diffraction (XRD), scanning electronic microscope (SEM), particle size analyzer (PSD), and thermal gravimetry analysis (TGA) were used to investigate the effect of ion-exchange techniques on the structure of the materials. CO_2 uptake of ZIF-67 ion exchanged by one-step method is much higher than that by the standard ion-exchange procedure. All of the adsorption isotherms show linear patterns with stable adsorption rate from 0 bar to 1 bar, which reveals the materials could get excellent adsorption performance at higher pressure range (>1 bar). Elemental analysis, N_2 physical adsorption, and the point of zero charge (PZC) were carried out to confirm the adsorption mechanism. van der Waals interaction determined by the surface area and coordination interaction resulting from electrostatic interaction work in synergy to enhance CO_2 adsorption performance of ZIF-67 ion exchanged by the one-step method.

1. Introduction

Zeolitic imidazolate frameworks (ZIFs) are a new class of porous materials constructed from coordinated divalent cations (e.g., Zn, Co) linked by imidazolate (Im) [1]. Many ZIFs have unusual high thermal and chemical stability for metalorganic frameworks [2, 3]. The well-known ZIF-8 is a prime example with a sodalite (SOD) topology, which can be boiled in water and other solvents without damage of the structure [4]. ZIF-67 is isostructural to ZIF-8 and is formed by linking 2-methylimidazolate anions and cobalt cations [5].

ZIFs have shown great potential applications in gas separation [6–8] and catalysis [9–11] because of their tunable zeotype topologies, high surface area, and metal content. To obtain ZIF adsorbents with large surface areas, adjustable pore sizes, open metal sites, and excellent CO_2 adsorption property, various functionalization techniques have been applied, such as functionalization with amine groups [12], specific functionalization of the imidazolate [13], isoreticular covalent functionalization [14, 15], formation of ZIF-inorganic substance composites [16], and cation exchange [17]. Among these functionalization methods, ion exchange could improve the surface area, pore volume, and surface charge of the adsorbents, further enhancing the CO_2 adsorption capacities. Lan et al. [18] found that Li was the best exchangeable cation of covalent organic frameworks (COFs) for CO_2 adsorption among alkali metal, alkaline-earth metal, and transition metal by the multiscale simulation approach.

A standard ion-exchange procedure was carried out as follows [19, 20]: the dried as-prepared sample was suspended in a 0.1 M sodium nitrate solution using an ethanol-water

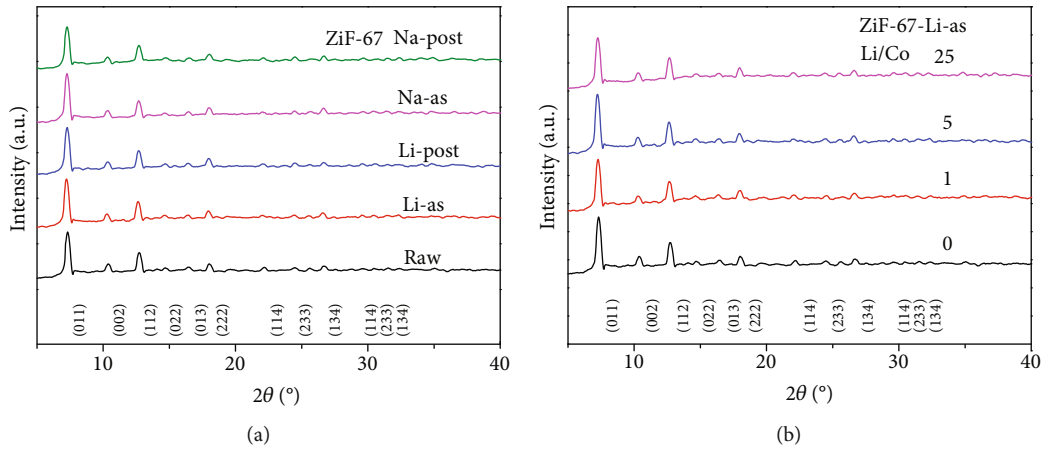

FIGURE 1: XRD patterns of ZIF-67. (a) Parent and exchanged with Li^+ and Na^+. (b) Parent and exchanged with different concentrations of Li^+.

mixture of molar ratio 3 : 1 and stirred at room temperature for 24 h. Obviously, the standard ion-exchange procedure could attributed to postsynthesis modification. And CO_2 uptake properties of the sorbents could be enhanced significantly [21, 22]. However, it is notable that the standard ion-exchange process needs to be repeated for several times, which brings a series of disadvantages, such as complicated in synthesis, time consuming, and solvent consuming.

In this work, we develop a new one-step ion-exchange method (donated as ion as-exchange technique) to overcome the disadvantages mentioned above. Since the cations for exchange were added before the hydrothermal preparation of ZIF-67, time consuming and solvent consuming in the standard ion-exchange procedure were eliminated. By comparison, the standard ion-exchange procedure was also carried out to synthesize the adsorbents. The structure, surface charge, and CO_2 adsorption properties of the adsorbents prepared via the two methods were investigated and compared.

2. Materials and Methods

2.1. Materials. All chemicals were analytic grade provided by Aladdin Chemical Reagent Co., Ltd., Shanghai, China.

2.2. Synthesis of the ZIF-67 and Ion-Exchanged ZIF-67. ZIF-67 was synthesized with the following procedure [23]. A solid mixture of $Co(NO_3)_2{\cdot}6H_2O$ (2.91 g, 10 mmol) and 2-methylimidazole (4.105 g, 50 mmol) was dissolved in methanol (150 ml) in a 200 ml Teflon liner with stirring. The Teflon liner was sealed with an autoclave and heated at 140°C for 72 h in a convection oven. After the product was cooled naturally to room temperature, chloroform was added to the product, and the crystals were collected from the upper layer. The crystals were immersed in methanol for 3 days and the solvent was exchanged with a fresh solvent daily.

The synthesis of ion-exchanged ZIF-67 was performed with ion as-exchange technique and ion post-exchanged technique (standard ion-exchange procedure).

Lithium nitrate ($LiNO_3$) or sodium nitrate ($NaNO_3$) was dissolved in the solutions containing $Co(NO_3)_2{\cdot}6H_2O$ and 2-methylimidazole. The synthesis and activation of ion as-exchanged ZIF-67 followed the same route of ZIF-67. The dark blue product was designated as M-as-n (mole ratio of $M : Co = 5$), where M represents the alkali metal ions (Li and Na); n represents the mole ratio of Li : Co ($n = 1$, 5 and 25).

In the synthesis of ion post-exchanged ZIF-67, dried as-prepared ZIF-67 was ion-exchanged with Li^+ and Na^+ cations. For this purpose, the as-prepared ZIF-67 was immersed in a solution of lithium and sodium chlorides in pure freshly distilled methanol, and stirred at room temperature for 24 h. The ion-exchange process was repeated 4 times. The dark blue product was obtained by filtration and drying, designated as M-post-5, where M represents the alkali metal ion (Li and Na); 5 represents the mole ratio of M : Co.

2.3. Characterization and Adsorption Measurements. The powder X-ray diffraction (XRD) (Beijing Purkinje General Instrument Co., Ltd., China) patterns were recorded using nickel-filtered Cu Kα radiation at 36 kV and 40 mA (2θ ranging from 5° to 80°, $\lambda = 0.15418$ nm and 0.02° step size). The morphologies and composition of samples were observed on the Hitachi-S4800 FESEM (Hitachi Electronics Co., Ltd., Japan) at an acceleration voltage of 30 kV. EDS mapping was applied to analyze the element extent and locate the elemental distribution on the surface of the materials. Metallic element (Co, Li and Na) was measured by OPTIMA 5300DV inductive-coupled plasma emission spectrometer (ICP-AES) (PerkinElmer Co. Ltd., Japan). The particle size distribution of the samples was measured using BT-9300S Laser Particle Size Analyzer (Dandong Bettersize Instrument Ltd., China) using water as dispersion medium. TG and DTG curves were obtained under oxygen atmosphere by Pyris 1 TGA heating from 30°C to 800°C at 20.00°C/min.

CO_2 adsorption isotherms were measured using a surface area and pore porosimetry analyzer (V-Sorb 2800P) under low pressure (0-1.1 bar). The experiments were conducted at 0°C by the Dewar flask using ice water or circulated water in which the sample tube was immersed. Prior to each adsorption experiment, the samples were degassed at 120°C

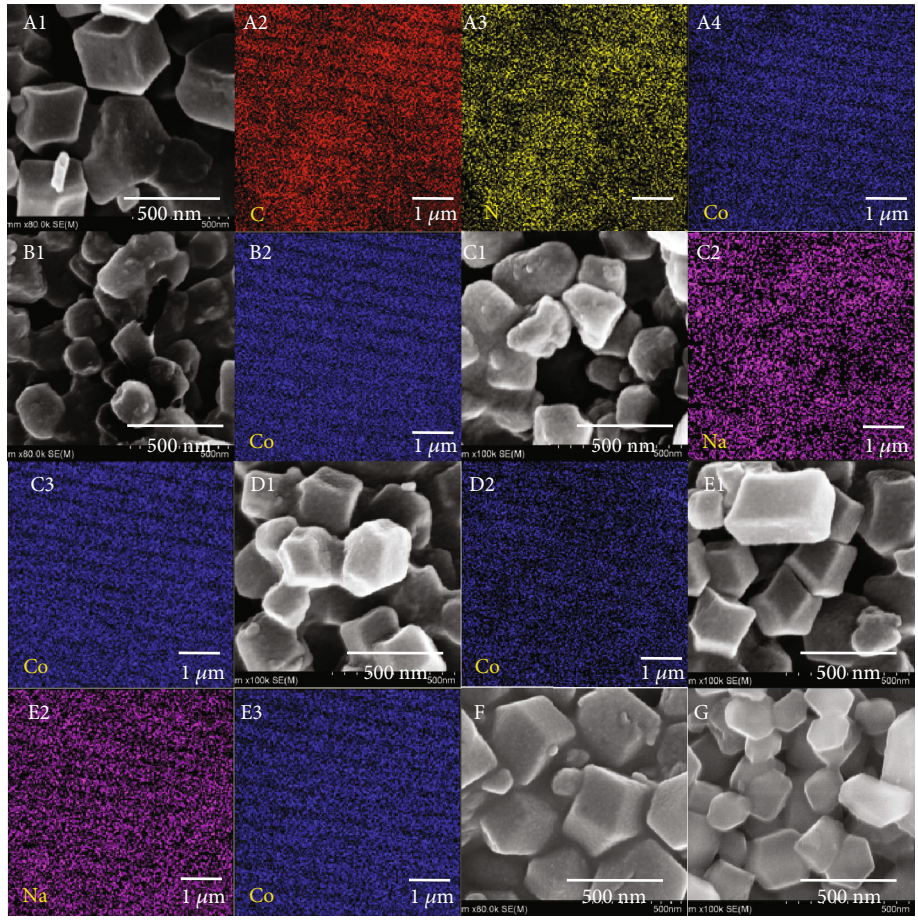

Figure 2: SEM-EDX mapping of ZIF-67. (a1–a4) SEM and EDX mapping of C, N, and Co for parent. (b1, b2, d1, d2) SEM and EDX mapping of Co for Li-post and Li-as (Li : Co = 5). (c1, c2, c3, e1, e2, e3) SEM and EDX mapping of Na and Co for Na-post and Na-as (M : Co = 5). (f, g) SEM of Li-as (f, Li : Co = 1; g, Li : Co = 25).

overnight. N_2 adsorption isotherms were measured using an ASAP 2020 analyzer (Micromeritics, Norcross, GA, USA) under low pressure (0-1.1 bar). The experiments were conducted at 0°C and 25°C. The reversibility of the CO_2 adsorption process on the samples studied was tested by multiple CO_2 adsorption cycles. The corresponding adsorption isotherms have been acquired after heating at 120°C for 12 h in vacuum in sequence.

The BET surface areas (S_{BET}) and pore volumes (V_{pore}) of given samples were determined by surface area and pore porosimetry analyzer (V-Sorb 2008P). The point of zero charge (pH_{PZC}) for the parent ZIF-67 and ion-exchanged ZIF-67 was estimated by a mass titration method [24]. After adsorption of CO_2 in the surface area analyzer mentioned above, pH_{PZC} of the adsorbents was measured with the same method.

3. Results and Discussion

Figure 1 shows the XRD patterns of ZIF-67 exchanged with Li^+ and Na^+ Figure 1(a) and that exchanged with different concentrations of Li^+ Figure 1(b). The diffraction pattern of parent ZIF-67 is in accordance with the data in the reported literature, indicating that the product was pure-phase ZIF-67 materials [25]. As shown in Figure 1(a), all the Li^+- and Na^+-exchanged ZIF-67 maintain crystallinity of the original phase. And almost no changes in peak intensity and position could be observed. Figure 1(b) reveals that the different Li^+-exchanged concentrations have no effect either on the crystallinity.

Table 1: Co, Li, and Na content of parent ZIF-67 and ion-exchanged ZIF-67 measured by SEM-EDX and ICP-AES.

ZIFs	Co (wt%)		Li (wt%)		Na (wt%)	
	EDX	ICP	EDX	ICP	EDX	ICP
Parent	9.22	28.24				
Li-as-5	5.36	25.67	—	0.66		
Na-as-5	6.50	26.15			3.46	1.94
Li-post-5	7.44	25.54	—	1.43		
Na-post-5	6.94	24.08			7.08	4.36

Figure 2 shows the scanning electron microscopy (SEM) images and EDX mapping of the parent and ion-exchanged ZIF-67 materials. As revealed in Figure 2(a1), the crystals of parent ZIFs are comprised of mostly regular multifaceted crystals with sharp edges and smooth surface [26]. The particle size is similar and around 300 nm. Ion-exchanged ZIF-67

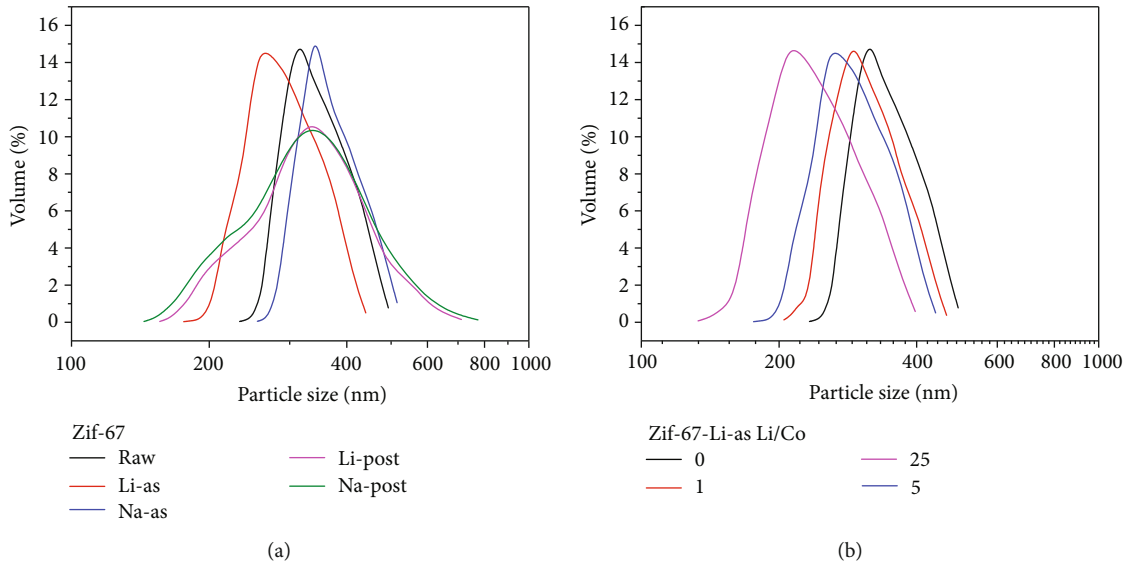

Figure 3: Particle size distribution of ZIF-67 samples. (a) Parent and post/as-exchanged (M : Co = 5). (b) Parent and as-exchanged with different concentrations of Li^+ (Li : Co = 1, 5, 25).

remains in the original polyhedral shape in various degrees. Most dramatically, Li^+- and Na^+-post-exchanged ZIFs (Figures 2(b1) and 2(c1)) tend to clump and agglomerate with smaller irregular polyhedral and tough surface because of the physical operations during the ion-post-exchanged procedure, such as stirring, while the as-exchanged samples (Figures 2(d1), 2(e1), 2(f), and 2(g)) maintain good dispersion and polyhedral shape. A change of the crystal sizes could be also observed. Na^+ as-exchanged ZIFs show an increase in the crystal size, while other ion-exchanged ZIFs show the decrease in crystal size with varying degrees. In addition, the particle sizes of Li^+ as-exchanged ZIFs decrease with the increase of ratio of $Li^+ : Co^{2+}$. Furthermore, the ZIF-67-Li-as-25 displayed the minimum crystal size, which is 200 nm approximately.

EDX mapping of parent ZIF-67 indicates that all C, N, and Co elements are dispersed uniformly on the surface of the materials. Similar situations occur in the EDX mapping of Co and Na for other ion-exchanged ZIFs, revealing that ion exchange may arise on the surface of the crystals evenly or randomly. The colour of Na element in Figure 2(c2) is much darker than that in Figure 2(e2), which probably proves that the Na content on the surface of Na-post-5 is higher than that of Na-as. Moreover, Li element is unable to be measured by EDX mapping since it is beyond the scope of the test method.

Element content of metallic element (Co, Li, and Na) on the surface and all over the material was measured by SEM-EDX and ICP-AES, respectively. As listed in Table 1, the Co content (wt%) of all the samples measured by EDX is much less than that by ICP, whereas the Na content test exhibits the opposite result. It indicates that the Co content on the surface of the crystals is less than its actual content. The ion exchange mainly occurred on the surface of the crystals. After the conversion of wt% to mol%, ICP result reveals that the mole ratios of M (Li or Na) : (M and Co) in M-as-5 are 17.89% and 15.91%, whereas that in M-post-5 are 32.19% and 31.72%. Most dramatically, M content in M-post is much higher than the content of reduced Co compared to the parent ZIF-67. Therefore, some M ions may physically deposit on the surface of the crystals rather than exchanging with Co ions.

Figure 3 presents the particle size distributions of as-synthesized and ion-exchanged ZIF-67 samples, which show the Gaussian-type distribution. The as-synthesized ZIF-67 crystals have an average particle size of 317 nm. After ion as-exchanged treatment, the average particle sizes of Li/Na-as-5 changed to 256 nm and 339 nm, respectively, which matches well with the trend of SEM observations (Figure 2). Dramatically, the particle size distributions of Li/Na-post-5 became broader, and the average particle sizes increased to 336 nm and 342 nm, respectively, which was in contrast with the trend of SEM results. It can be attributed to the agglomerate phenomenon observed from Figure 2. As seen from Figure 3(b), the average particle sizes of Li-as-1/5/25 were 289 nm, 256 nm, and 213 nm, respectively, decreasing with the increase of ratio of $Li^+ : Co^{2+}$.

3.1. Adsorption Studies. The corresponding CO_2 adsorption isotherms of parent and these ion-exchanged ZIFs are shown in Figure 4(a). At 0°C, the CO_2 uptake of parent ZIF-67 at 1 bar is 35.4 cm^3/g. Li/Na-post-5 exhibited decreased CO_2 adsorption capacity (30.4 and 31.2 cm^3/g) compared to the parent, while Li/Na-as-5 showed improved CO_2 uptake values (48.7 and 45.1 cm^3/g). The highest CO_2 capacity is achieved by Li-as-5, which is 37.6% higher than that of the parent ZIF-67. At 250°C, the CO_2 uptakes on ZIF samples follow the similar order. The decreases in adsorption amount of post-exchanged ZIFs were correlated with the clump and agglomerate (Figures 2(b) and 2(c)). This phenomenon may lead to a decrease in pore volume and adsorption sites, which was extremely similar to the effect of carbon deposition behavior on pore volume [27, 28]. In Figure 4(b), the CO_2 uptake of Li-as-*n* with varying $Li^+ : Co^{2+}$ ratios at 1 bar

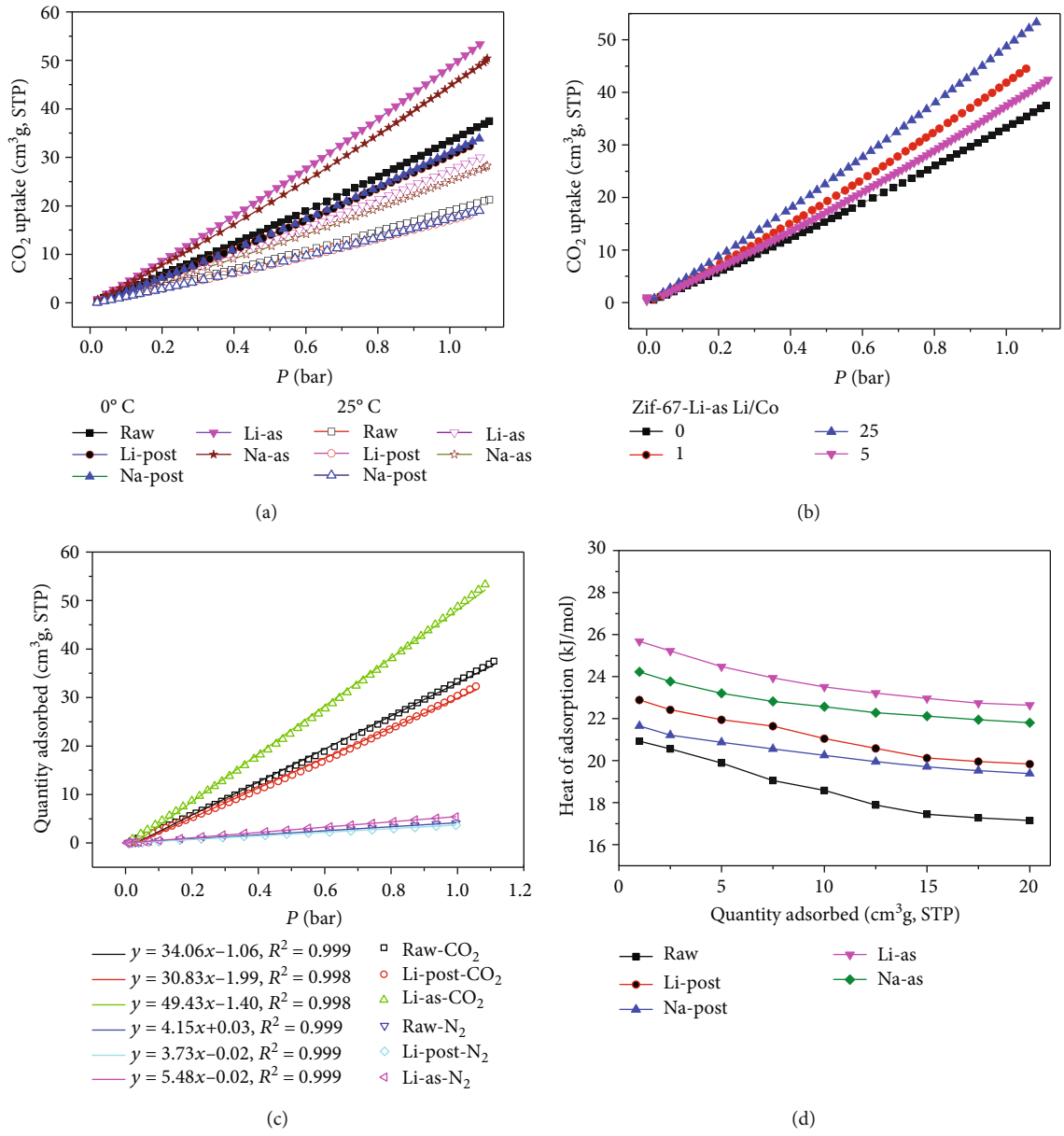

FIGURE 4: (a) The CO_2 adsorption isotherms of ZIF-67 samples: parent and post/as-exchanged (M : Co = 5) at 0°C and 25°C. (b) The CO_2 adsorption isotherms of parent ZIF-67 and as-exchanged with different concentrations of Li^+. (c) The CO_2/N_2 adsorption isotherms of ZIF-67 samples and corresponding linear fit results. (d) Heat of adsorption for CO_2 calculated in ZIF-67 samples.

was 41.8, 48.7, and 37.6 cm^3/g, respectively, which could not be directly correlated with the amounts of Li^+. An interesting phenomenon is found that all of the isotherms show linear patterns with stable adsorption rate from 0 bar to 1 bar, which could be attributed to monomolecular adsorption (Henry-type model). It reveals the materials could get excellent adsorption performance at higher pressure range (>1 bar).

The CO_2/N_2 adsorption isotherms of parent ZIF-67, Li-post-5, and Li-as-5 are collected in Figure 4(c) to calculate the CO_2/N_2 selectivity. The N_2 uptakes of the 3 samples follow the order of their CO_2 uptake. The corresponding linear fit results are also shown in Figure 4(c). The CO_2/N_2 selectivity could be calculated by the ratio of Henry coefficient, which is equal to the slope of the isotherms after linear fit. Therefore, S (CO_2/N_2) of parent ZIF-67, Li-post-5, and Li-as-5 is 18.21, 18.27, and 19.02, respectively, showing a good selectivity for CO_2/N_2 separation.

The interaction of guest molecules with host materials is usually evaluated by the isosteric heat of adsorption ΔH_{ads} [29, 30]. Figure 4(d) shows that the ΔH_{ads} on ZIF-67 for CO_2 follows the following order: Li-as > Na-as > Li-post > Na-post > parent, which was different from the order of their CO_2 uptakes. It is suggested that the dispersion of the Li and Na species can create a high electric field on the surface of ZIF, leading to a higher binding force with quadrupolar CO_2 molecules [31].

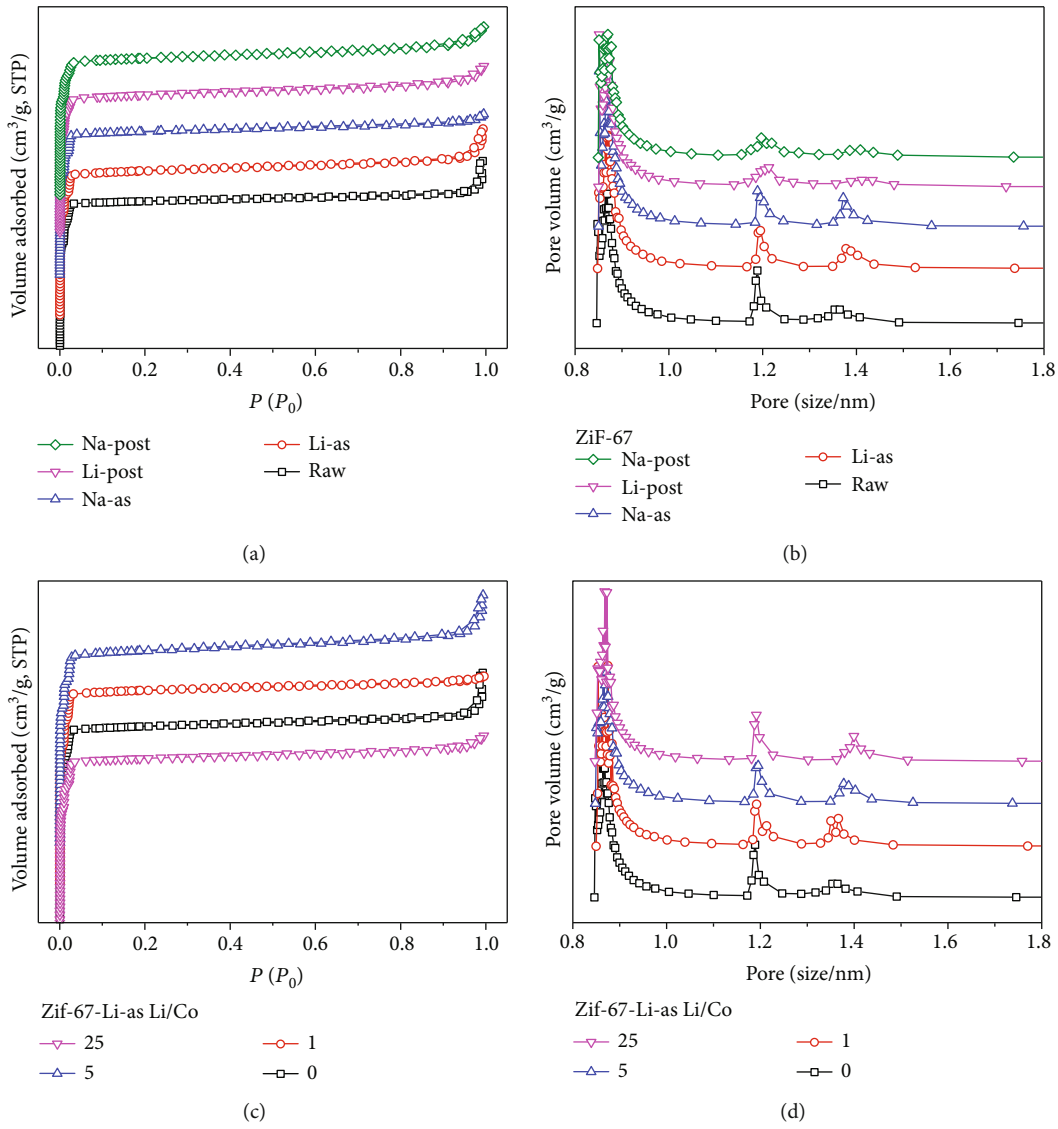

Figure 5: Nitrogen sorption isotherms and pore size distribution of ZIF-67 samples. (a, b) Parent and post/as-exchanged (M : Co = 5). (c, d) Parent and as-exchanged with different concentrations of Li^+ (Li : Co = 1, 5, 25).

Table 2: Physical properties of parent ZiF-67 and ion-exchanged ZiF-67.

ZiFs	BET (m^2/g)	Pore volume (m^3/g)	SF median pore width (nm)
Parent	1424.59	0.84	0.868
Li-as-5	1450.71	0.87	0.875
Na-as-5	1435.15	0.86	0.871
Li-post-5	1366.14	0.76	0.851
Na-post-5	1359.50	0.77	0.864

Table 3: Physical properties of parent ZIF-67 and Li-as-exchanged ZIF-67 with varying $Li^+ : Co^{2+}$ ratios.

ZIFs	BET (m^2/g)	Pore volume (m^3/g)	SF median pore width (nm)
Parent	1424.59	0.84	0.868
Li-as-1	1432.34	0.86	0.873
Li-as-5	1450.71	0.87	0.875
Li-as-25	1353.96	0.71	0.868

3.2. CO_2 Adsorption Mechanism. To confirm the reason for varying CO_2 adsorption capacities of ion-exchanged ZIFs, low temperature N_2 adsorption and PZC characterization were carried out.

N_2 adsorption isotherms and pore size distributions of the parent and ion-exchanged ZIF-67 materials are shown in Figure 5. Physical properties of these materials are listed in Table 2 and Table 3. As revealed in Figure 5(a), the isotherm of parent ZIF-67 reveals typical type I behavior as expected for microporous materials, corresponding to that

reported in the literatures [32, 33]. The surface area, pore volume, and SF median pore width are 1424.59 m^2/g, 0.84 cm^3/g, and 0.868 nm, respectively. As shown in Figure 5(b), the pore size of parent ZIF-67 was distributed at 0.86, 1.18, and 1.36 nm.

The entire ion-exchanged ZIFs maintained type I isotherms and similar pore size distribution with a right shift, while the pore volumes of Li/Na-post-5 decreased dramatically. As shown in Table 2, the surface area, pore volume, and SF median pore width of Li/Na-as-5 increase significantly, while those of post-exchanged materials decrease contrarily. It was reported that the standard ion-exchange procedure could improve the surface area and pore volume [34], which was opposite to our results. As can be seen from Figure 5(b), although the second pore size distribution peak of Li/Na-post-5 shifts from 1.18 nm to 1.21 nm and 1.20 nm, respectively, their peak height decreases significantly, indicating a decrease of pore volume. That is because the concentration of exchanged ions in our procedure is much higher than that in the standard ion-exchange procedure. A small quantity of Li^+ or Na^+ with smaller radius replaced Co^{2+} of ZIF-67, leading to an expanded pore size as mentioned above. However, other Li^+/Na^+ remained in the pores or attached on the surface, resulting in agglomerate and pore block.

The N_2 adsorption isotherms and pore size distribution of the parent and as-exchanged ZIF-67 with different concentrations of Li^+ are collected in Figures 5(c) and 5(d). Their physical properties are listed in Table 3. The surface area and pore volume of Li-as-exchanged sample ($Li^+/Co^{2+} = 5$) are 1450.71 cm^2/g and 0.84 cm^3/g, which is the highest value among all the samples. When the $Li^+ : Co^{2+}$ ratio increased to 25, surface area and pore volume declined to 1353.96 cm^2/g and 0.71 cm^3/g. Therefore, the Li^+ ion as-exchange technique enhanced the surface area and pore volume to the greatest extent. And the optimal $Li^+ : Co^{2+}$ ratio is 5.

The position of the PZC defines the affinity of the surface of the adsorbents to the adsorbate. Therefore, determination of the PZC is an important element of the characterization of adsorbents [35]. In order to study the influence of ion-exchange procedures and exchanged ion species on the acid-base properties of the ZIF-67 surfaces, the point of zero charge (pH_{PZC}) was estimated by a mass titration method. The pH_{PZC} values of the parent ZIF-67 and ion-exchanged ZIF-67 before and after CO_2 adsorption are listed in Table 4 and Table 5.

As shown in Table 4, parent ZIF-67 has a neutral character with pH_{PZC} value of 6.92, whereas ion-exchanged ZIF_S have basic surfaces (pH_{PZC} values ranging from 7.51-9.26). Obviously, pH_{PZC} values of Li^+ and Na^+ as-exchanged ZIFs are higher than those of post-exchanged samples. And Li-as exhibits the highest pH_{PZC} value of 9.26, indicating that ion as-exchange technique with Li^+ could enhance the surface basicity of the adsorbents to the greatest degree. The pH_{PZC} values of all samples decreased to the range of 5.10-5.63 after CO_2 adsorption. In Table 5, pH_{PZC} values of Li^+ as-exchanged ZIFs increased with the increase of $Li^+ : Co2^+$ ratios. After CO_2 adsorption, pH_{PZC} decreased to the range of 5.14-5.42 similarly as before.

Table 4: The pH_{PZC} values of the parent ZIF-67 and ion-exchanged ZIF-67 before and after CO_2 adsorption.

Sample	pH_{PZC} values	
	Before CO_2 adsorption	After CO_2 adsorption
Parent	6.92	5.36
Li-post-5	7.79	5.10
Na-post-5	7.51	5.63
Li-as-5	9.26	5.27
Na-as-5	8.83	5.49

Table 5: The pH_{PZC} values of the parent ZIF-67 and Li-as-exchanged ZIF-67 with varying $Li^+ : Co^{2+}$ ratios before and after CO_2 adsorption.

Sample	pH_{PZC} values	
	Before CO_2 adsorption	After CO_2 adsorption
Parent	6.92	5.36
Li-as-1	8.49	5.14
Li-as-5	9.26	5.27
Li-as-25	9.31	5.42

The mechanism of CO_2 adsorption on the parent and Li^+/Na^+ as-exchanged ZIF-67 is deduced in Figure 6. Because the radius of Li^+ and Na^+ was smaller than that of Co^{2+}, the Li^+/Na^+ ion as-exchange technique enhanced the surface area and pore volume. Li^+ has a smaller radius compared with Na^+; thus, ZIF-67-Li-as shows the highest surface area and pore volume. As mentioned above, the order of CO_2 uptake of the samples is consistent with that of surface area. It confirmed that CO_2 adsorption on the synthesized adsorbents is dependent on van der Waals interaction determined by the surface area to a great degree.

According to the hard and soft acid-base principle (HASB principle), both Li^+ and Na^+ in ZIFs could be regarded as Lewis acid with strong attractive force on outer electrons. They could coordinate with CO_2 considered as a kind of Lewis base, which improved CO_2 adsorption. And the coordination interaction mainly results from electrostatic interaction [36]. Since Li^+ has a larger radius to charge ratio compared with Na^+, Li^+ cation owns strong quadrupole moment (ΦFQ), further enhancing the strong affinity of Li^+ ions for CO_2 molecules. According to Kumar et al.'s report [16], the CO_2 adsorption capacity in ion-exchanged sod-ZMOF appears to depend not only on the size and charge of the balancing cations but also on the distribution of the cations located in the framework structures, which is not exactly known at present. In short, van der Waals interaction determined by the surface area and coordination interaction resulting from electrostatic interaction work in synergy to enhance CO_2 adsorption. Although the adsorbent prepared via the post ion-exchange method contains more Li^+/Na^+ cations, the pore volumes decreased dramatically due to the agglomerate and pore block by excessive cations. Synergistic effects lead to worse CO_2 adsorption properties on Li-post and Na-post.

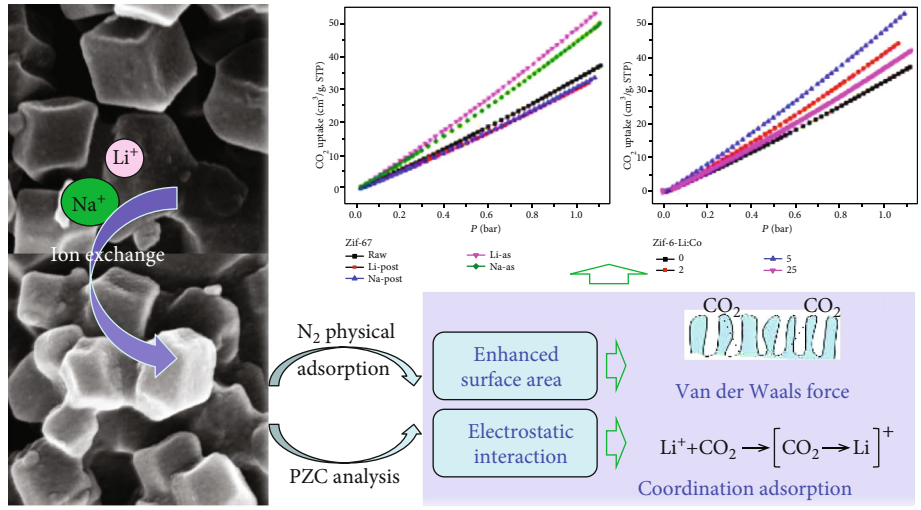

Figure 6: The mechanism of CO_2 adsorption on Li^+ and Na^+ as-exchanged ZIFs.

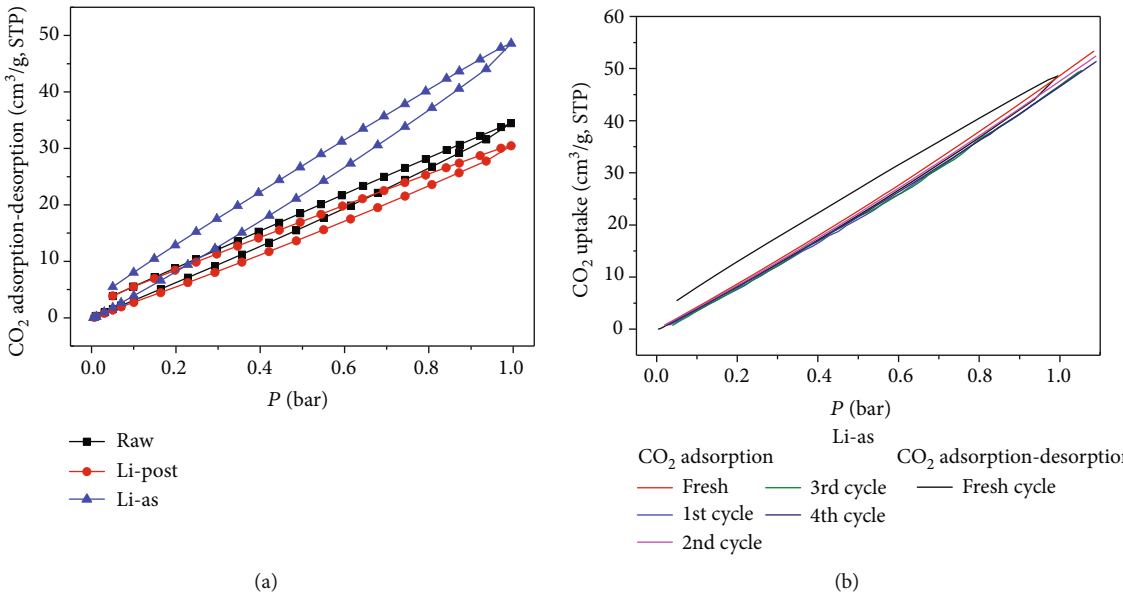

Figure 7: (a) CO_2 adsorption-desorption isotherms measured at 0°C. (b) CO_2 recycle performance (adsorption at 0°C and desorption at 120°C) and CO_2 adsorption-desorption isotherms of Li-as-5 (measured at 0°C) of Li-as.

3.3. CO_2 Adsorption-Desorption Isotherms and Cyclic Adsorption-Regeneration Test. Figure 7(a) depicts the CO_2 adsorption-desorption isotherms of parent ZIF-67, Li-post-5, and Li-as-5 at 0°C. Dramatically, all of the 3 desorption isotherms lag behind the corresponding adsorption isotherms, with a small quantity of undesorbed CO_2 left in the adsorbents after the desorption process. Because the desorption isotherms were carried out from 1 bar to 0.05 bar, the adsorbed CO_2, undesorbed CO_2 at 0.05 bar, and other related parameters are listed in Table 6 to analyze the adsorption-desorption performance. The decrement of parent ZIF-67, Li-post-5, and Li-as-5 is 6.7%, 8.3%, and 7.6%, respectively, corresponding to the chemically adsorbed CO_2 by coordination interaction.

Figure 7(b) depicts the CO_2 adsorption-regeneration cycle of Li-as-5 in consideration of its optimal adsorption capacity. The regeneration was performed at 120°C in vacuum in sequence. The adsorption/regeneration cycle was repeated for a total of 4 cycles. And the cyclic CO_2 adsorption capacities of the 4 cycles at 1 bar are 47.3 cm^3/g, 48.0 cm^3/g, 47.7 cm^3/g, and 46.9 cm^3/g, respectively. The decrement of cyclic CO_2 adsorption after regeneration at 120°C in vacuum is in the range of 1.4%-3.7%. However, the decrement of CO_2 adsorption-desorption isotherms (desorbed at 0°C) is 7.6% as mentioned above. The former decrement was smaller than the latter decrement; that is to say, most of the undesorbed CO_2 of Li-as-5 at 0°C (chemically adsorbed CO_2 by coordination interaction) could be desorbed at 120°C in vacuum. It

Table 6: Analysis results of CO_2 adsorption-desorption isotherms measured at 0°C.

ZIFs	Adsorbed CO_2 at 0.05 bar (cm^3/g)	Undesorbed at 0.05 bar (cm^3/g)	△(Un-Ad)[1] (cm^3/g)	Adsorbed CO_2 at 1.0 bar (cm^3/g)	Decrement (%)
Raw	1.56	3.87	2.31	34.44	6.7
Li-post	1.38	3.91	2.53	30.48	8.3
Li-as	1.78	5.48	3.70	48.57	7.6

[1]△(Un-Ad) represents the differentials between the value of desorption and adsorption isotherms at 0.05 bar.

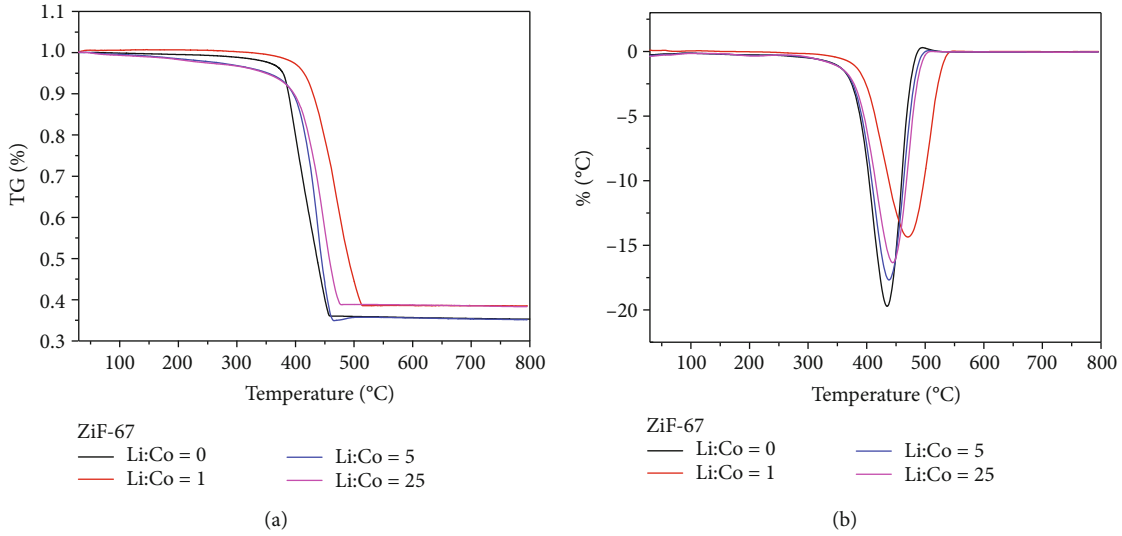

Figure 8: TG (a) and DTG (b) curves of ZIF-67 and Li-as-exchanged ZIF-67 with varying $Li^+ : Co^{2+}$ ratios.

indicated that the CO_2 coordination adsorption on Li-as was weak and almost reversible at a higher temperature in vacuum, similar to the chemisorptions of CO_2 on amine-functionalized adsorbents [37, 38].

3.4. Thermal Stability Characterized by TGA. TG and DTG curves of ZIF-67 and Li-as-exchanged ZIF-67 with varying $Li^+ : Co^{2+}$ ratios are collected in Figure 8(a) and Figure 8(b), respectively. As shown in Figure 8(a), ZIF-67 shows that only 2.3% weight loss up to 350°C, corresponding to the removal of guest molecules and unreacted species [39]. Thus, the ZIF-67 material is thermally stable below 350°C at O_2 atmosphere. Although the thermal stability of ZIF-67 is slightly lower than that of ZIF-8 (ca. 500°C) [40], it still surpasses most of MOF materials [41]. The thermal stability of Li^+ ion as-exchanged samples was improved in various degrees. The Li-as-exchanged materials with $Li^+ : Co^{2+}$ ratio of 5 and 25 enhanced its thermostability slightly, while that of $Li^+ : Co^{2+}$ ratio of 1 was improved dramatically, which could be thermally stable up to 390°C. Accordingly, a similar trend can be informed in the DTG curves of Figure 8(b). The weight loss rate of Li^+ ion as-exchanged samples decreased in varying degrees and the weight loss peaks shifted to higher temperature, indicating that the Li^+ ion as-exchange technique improved the thermal stability of ZIF-67 materials. In addition, it was observed that sharp turning points of unit decomposition in TG and DTG curves, as the curves were obtained under O_2 atmosphere, which accelerate the decomposition of the samples. When O_2 atmosphere was replaced by N_2 atmosphere, the turning points became smoother. Similar results were obtained by Chen et al.'s study [42].

4. Conclusions

Li^+- and Na^+-exchanged ZIF-67 was synthesized by a new one-step method of ion as-exchange technique for CO_2 capture. By comparison, the standard ion-exchange procedure of ion post-exchanged technique was also carried out. The structure, surface charge, and CO_2 adsorption properties and mechanism of the adsorbents prepared via the two methods were investigated. The surface area and pore volume of Li^+/Na^+ as-exchanged ZIF-67 increase significantly because the radius of Li^+ and Na^+ is smaller than that of Co^{2+}. And the optimal $Li^+ : Co^{2+}$ ratio is 5. However, the surface area of post-exchanged materials decreases contrarily due to the agglomerate and pore block, which could be proved by SEM and particle size distribution results. PZC characterization indicates that parent ZIF-67 has a neutral character, whereas ion-exchanged ZIFs have basic surfaces. And pH_{PZC} values of Li^+ and Na^+ as-exchanged ZIFs are higher than those of post-exchanged samples, which could improve CO_2 adsorption due to the coordination interaction. All of the CO_2 adsorption isotherms show linear patterns with stable adsorption rate from 0 bar to 1 bar, which reveals the materials could get excellent adsorption performance at

higher pressure range (>1 bar). van der Waals interaction determined by the surface area and coordination interaction resulting from electrostatic interaction work in synergy to enhance CO_2 adsorption performance of Li^+/Na^+ as-exchanged ZIF-67 adsorbents.

Data Availability

The data used to support the findings of this study are included within the article.

Disclosure

A conference abstract entitled "A one-step ion exchange method to functionalized ZiF-67 for enhanced CO_2 capture" has been presented in 2016 AIChE Annual Meeting in the following link: https://aiche.confex.com/aiche/2016/webprogram/Paper454249.html. The abstract only published the preliminary or partial results of scientific research without detailed results and discussion, and a large number of other data in this manuscript have not been published.

Conflicts of Interest

The authors declare that they have no conflicts of interest.

Authors' Contributions

Dr. Qin Zhong has made a significant scientific contribution to the manuscript.

Acknowledgments

Specially, we would like to thank Dr. Qin Zhong from Nanjing University of Science and Technology for providing some testing instruments and revising the manuscript. In addition, we would like to thank Dr. Wei Chu from Sichuan University in consideration of Professor Chu Wei's guidance in the revision of the paper. This work was supported by the Joint Open Fund of Jiangsu Collaborative Innovation Center for Ecological Building Material and Environmental Protection Equipment and Key Laboratory for Advanced Technology in Environmental Protection of Jiangsu Province, under Construction for Volatile Organic Compounds Controlling of Jiangsu Province. This work was also supported by funding for school-level research projects of Yancheng Institute of Technology (154203639).

References

[1] K. Ishaq, B. Mohammed, B. Saleh et al., "Morphology controlled porous poly(lactic acid)/zeolitic imidazolate framework-8 fibrous membranes with superior PM2.5 capture capacity," *Chemical Engineering Journal*, vol. 338, pp. 82–91, 2018.

[2] G. Xiao, Y. Wang, and T. Kuang, "ZIF-8 based membranes for carbon dioxide capture/separation," *ACS Sustainable Chemistry & Engineering*, vol. 5, no. 12, pp. 11204–11214, 2017.

[3] A. Barjola, J. Escorihuela, A. Andrio, E. Giménez, and V. Compañ, "Enhanced conductivity of composite membranes based on sulfonated poly (ether ether ketone) (SPEEK) with zeolitic imidazolate frameworks (ZIFs)," *Nanomaterials*, vol. 8, no. 12, pp. 1042–1058, 2018.

[4] T. Wu, X. Feng, S. K. Elsaidi, P. K. Thallapally, and M. A. Carreon, "Zeolitic imidazolate framework-8 (ZIF-8) membranes for Kr/Xe separation," *Industrial & Engineering Chemistry Research*, vol. 56, no. 6, pp. 1682–1686, 2017.

[5] R. Banerjee, A. Phan, B. Wang et al., "High-throughput synthesis of zeolitic imidazolate frameworks and application to CO_2 capture," *Science*, vol. 319, no. 5865, pp. 939–943, 2008.

[6] Y. Gao, Z. Qiao, S. Zhao, Z. Wang, and J. Wang, "In situsynthesis of polymer grafted ZIFs and application in mixed matrix membrane for CO2separation," *Journal of Materials Chemistry A*, vol. 6, no. 7, pp. 3151–3161, 2018.

[7] J. An and N. L. Rosi, "Tuning MOF CO_2 adsorption properties via cation exchange," *Journal of the American Chemical Society*, vol. 132, no. 16, pp. 5578-5579, 2010.

[8] P. Krokidas, M. Castier, and I. G. Economou, "Computational study of ZIF-8 and ZIF-67 performance for separation of gas mixtures," *Journal of Physical Chemistry C*, vol. 121, no. 33, pp. 17999–18011, 2017.

[9] H. Yang, X. W. He, F. Wang, Y. Kang, and J. Zhang, "Doping copper into ZIF-67 for enhancing gas uptake capacity and visible-light-driven photocatalytic degradation of organic dye," *Journal of Materials Chemistry*, vol. 22, no. 41, pp. 21849–21851, 2012.

[10] T. T. Isimjan, H. Kazemian, S. Rohani, and A. K. Ray, "Photocatalytic activities of Pt/ZIF-8 loaded highly ordered TiO_2 nanotubes," *Journal of Materials Chemistry*, vol. 20, no. 45, pp. 10241–10245, 2010.

[11] C. Han, C. Zhang, N. Tymińska, J. R. Schmidt, and D. S. Sholl, "Insights into the stability of zeolitic imidazolate frameworks in humid acidic environments from first-principles calculations," *Journal of Physical Chemistry C*, vol. 122, no. 8, pp. 4339–4348, 2018.

[12] A. Huang, Q. Liu, N. Wang, and J. Caro, "Organosilica functionalized zeolitic imidazolate framework ZIF-90 membrane for CO_2/CH_4 separation," *Microporous and Mesoporous Materials*, vol. 192, no. 3, pp. 18–22, 2014.

[13] H. Hayashi, A. P. Côté, H. Furukawa, M. O'Keeffe, and O. M. Yaghi, "Zeolite A imidazolate frameworks," *Nature Materials*, vol. 6, no. 7, pp. 501–506, 2007.

[14] Z. Wang and S. M. Cohen, "Postsynthetic modification of metal-organic frameworks," *Chemical Society Reviews*, vol. 38, no. 5, pp. 1315–1329, 2009.

[15] M. J. Ingleson, J. Perez Barrio, J.-B. Guilbaud, Y. Z. Khimyak, and M. J. Rosseinsky, "Framework functionalisation triggers metal complex binding," *Chemical Communications*, vol. 23, no. 23, pp. 2680–2682, 2008.

[16] R. Kumar, K. Jayaramulu, T. K. Maji, and C. N. Rao, "Hybrid nanocomposites of ZIF-8 with graphene oxide exhibiting tunable morphology, significant CO_2 uptake and other novel properties," *Chemical Communications*, vol. 49, no. 43, pp. 4947–4949, 2013.

[17] C. Chen, J. Kim, D.-A. Yang, and W.-S. Ahn, "Carbon dioxide adsorption over zeolite-like metal organic frameworks (ZMOFs) having a *sod* topology: Structure and ion-exchange effect," *Chemical Engineering Journal*, vol. 168, no. 3, pp. 1134–1139, 2011.

[18] J. Lan, D. Cao, W. Wang, and B. Smit, "Doping of alkali, alkaline-earth, and transition metals in covalent-organic frameworks for enhancing CO_2 capture by first-principles calculations and molecular simulations," *ACS Nano*, vol. 4, no. 7, pp. 4225–4237, 2010.

[19] H. Fei, J. F. Cahill, K. A. Prather, and S. M. Cohen, "Tandem postsynthetic metal ion and ligand exchange in zeolitic imidazolate frameworks," *Inorganic Chemistry*, vol. 52, no. 7, pp. 4011–4016, 2013.

[20] F. Nouar, J. Eckert, J. Eubank, P. Forster, and M. Eddaoudi, "Zeolite-like metal-organic frameworks (ZMOFs) as hydrogen storage platform: lithium and magnesium ion-exchange and H(2)-(rho-ZMOF) interaction studies," *Journal of the American Chemical Society*, vol. 131, no. 8, pp. 2864–2870, 2009.

[21] K. S. Walton, M. B. Abney, and M. Douglas LeVan, "CO_2 adsorption in Y and X zeolites modified by alkali metal cation exchange," *Microporous and Mesoporous Materials*, vol. 91, no. 1-3, pp. 78–84, 2006.

[22] L. Zhang, J. N. Primera-Pedrozo, and A. J. Hernández-Maldonado, "Thermal detemplation of Na-SAPO-34: effect on Sr^{2+} Ion exchange and CO_2 Adsorption," *Journal of Physical Chemistry C*, vol. 114, no. 35, pp. 14755–14762, 2010.

[23] R. Chen, J. Yao, Q. Gu et al., "A two-dimensional zeolitic imidazolate framework with a cushion-shaped cavity for CO_2 adsorption," *Chemical Communications*, vol. 49, no. 82, pp. 9500–9502, 2013.

[24] T. Karanfil and J. E. Kilduff, "Role of granular activated carbon surface chemistry on the adsorption of organic compounds. 1. Priority pollutants," *Environmental Science & Technology*, vol. 33, no. 18, pp. 3217–3224, 1999.

[25] J. Qian, F. Sun, and L. Qin, "Hydrothermal synthesis of zeolitic imidazolate framework-67 (ZIF-67) nanocrystals," *Materials Letters*, vol. 82, pp. 220–223, 2012.

[26] A. F. Gross, E. Sherman, and J. J. Vajo, "Aqueous room temperature synthesis of cobalt and zinc sodalite zeolitic imidizolate frameworks," *Dalton Transactions*, vol. 41, no. 18, pp. 5458–5460, 2012.

[27] N. Maes and E. F. Vansant, "Modification of the porosity of pillared clays by carbon deposition II. Hydrocarbon cracking," *Journal of Porous Materials*, vol. 4, no. 1, pp. 5–15, 1997.

[28] Y. Yang, W. Z. Li, and H. Y. Xu, "Influence of CeO_2 and Co_3O_4 promoters on carbon deposition and carbon elimination over Ni-based catalysts," *Chinese Journal of Catalysis*, vol. 23, no. 6, pp. 517–520, 2002.

[29] G. Wang, B. Dou, Z. Zhang, J. Wang, H. Liu, and Z. Hao, "Adsorption of benzene, cyclohexane and hexane on ordered mesoporous carbon," *Journal of Environmental Sciences*, vol. 30, pp. 65–73, 2015.

[30] H. Ma, H. Ren, X. Zou et al., "Novel lithium-loaded porous aromatic framework for efficient CO_2 and H_2 uptake," *Journal of Materials Chemistry A*, vol. 1, no. 3, pp. 752–758, 2013.

[31] A. J. Hernandez-Maldonado, J. Guerrero-Medina, and V. C. Arce-Gonzalez, "Long range structural and textural changes in [Zn(bdc)(ted) 0.5] upon spontaneous dispersion of LiCl and hysteretic adsorption and desorption of carbon dioxide and hydrogen," *Journal of Materials Chemistry A*, vol. 1, no. 6, pp. 2343–2350, 2013.

[32] J. Yao, M. He, K. Wang, R. Chen, Z. Zhong, and H. Wang, "High-yield synthesis of zeolitic imidazolate frameworks from stoichiometric metal and ligand precursor aqueous solutions at room temperature," *CrystEngComm*, vol. 15, no. 18, pp. 3601–3606, 2013.

[33] X. Feng and M. A. Carreon, "Kinetics of transformation on ZIF-67 crystals," *Journal of Crystal Growth*, vol. 418, pp. 158–162, 2015.

[34] G. Calleja, J. A. Botas, M. Sánchez-Sánchez, and M. G. Orcajo, "Hydrogen adsorption over zeolite-like MOF materials modified by ion exchange," *International Journal of Hydrogen Energy*, vol. 35, no. 18, pp. 9916–9923, 2010.

[35] M. Kosmulski, "The pH-dependent surface charging and the points of zero charge," *Journal of Colloid and Interface Science*, vol. 253, no. 1, pp. 77–87, 2002.

[36] H. Zhuo, Q. Li, W. Li, and J. Cheng, "The dual role of pnicogen as Lewis acid and base and the unexpected interplay between the pnicogen bond and coordination interaction in $H_3N \cdots FH_2X \cdots MCN$ ($X = P$ and As; $M = Cu, Ag$, and Au)," *New Journal of Chemistry*, vol. 39, no. 3, pp. 2067–2074, 2015.

[37] Q. Liu, J. Shi, S. Zheng, M. Tao, Y. He, and Y. Shi, "Kinetics studies of CO_2 Adsorption/Desorption on amine-functionalized multiwalled carbon nanotubes," *Industrial & Engineering Chemistry Research*, vol. 53, no. 29, pp. 11677–11683, 2014.

[38] X. Wang, L. Chen, and Q. Guo, "Development of hybrid amine-functionalized MCM-41 sorbents for CO_2 capture," *Chemical Engineering Journal*, vol. 260, pp. 573–581, 2015.

[39] J. Cravillon, S. Münzer, S.-J. Lohmeier, A. Feldhoff, K. Huber, and M. Wiebcke, "Rapid room-temperature synthesis and characterization of nanocrystals of a prototypical zeolitic imidazolate framework," *Chemistry of Materials*, vol. 21, no. 8, pp. 1410–1412, 2009.

[40] Y. Pan, Y. Liu, G. Zeng, L. Zhao, and Z. Lai, "Rapid synthesis of zeolitic imidazolate framework-8 (ZIF-8) nanocrystals in an aqueous system," *Chemical Communications*, vol. 47, no. 7, pp. 2071–2073, 2011.

[41] K. K. Gangu, S. Maddila, S. B. Mukkamala, and S. B. Jonnalagadda, "Characteristics of MOF, MWCNT and graphene containing materials for hydrogen storage: a review," *Journal of Energy Chemistry*, vol. 30, pp. 132–144, 2019.

[42] E. X. Chen, H. Yang, and J. Zhang, "Zeolitic imidazolate framework as formaldehyde gas sensor," *Inorganic Chemistry*, vol. 53, no. 11, pp. 5411–5413, 2014.